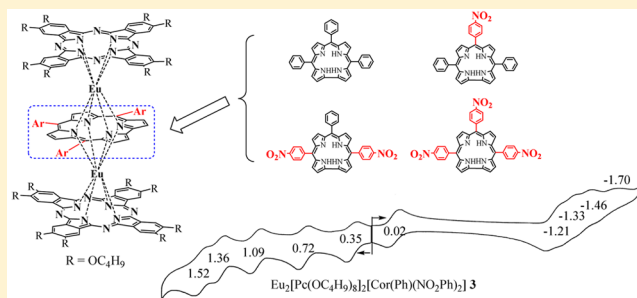


Europium Triple-Decker Complexes Containing Phthalocyanine and Nitrophenyl–Corrole Macrocycles

Guifen Lu,^{*,†,‡} Jing Li,[†] Xiaoqin Jiang,[‡] Zhongping Ou,[†] and Karl M. Kadish^{*,‡}[†]School of Chemistry and Chemical Engineering, Jiangsu University, Zhenjiang 212013, P. R. China[‡]Department of Chemistry, University of Houston, Houston, Texas 77204-5003, United States

Supporting Information

ABSTRACT: A series of europium triple-decker complexes containing phthalocyanine and nitrophenyl–corrole macrocycles were synthesized and characterized by spectroscopic and electrochemical methods in nonaqueous media. The examined compounds are represented as $\text{Eu}_2[\text{Pc}(\text{OC}_4\text{H}_9)_8]_2[\text{Cor}(\text{Ph})_n(\text{NO}_2\text{Ph})_{3-n}]$, where n varies from 0 to 3, $\text{Pc}(\text{OC}_4\text{H}_9)_8$ represents the phthalocyanine macrocycle, and Cor indicates the corrole macrocycle having phenyl (Ph) or nitrophenyl (NO_2Ph) meso substituents. Three different methods were used for syntheses of the target complexes, two of which are reported here for the first time. Each examined compound undergoes five reversible one-electron oxidations and 3–5 one-electron reductions depending upon the number of NO_2Ph substituents. The nitrophenyl groups on the meso positions of the corrole are highly electron-withdrawing, and this leads to a substantial positive shift in potential for the five oxidations and first reduction in CH_2Cl_2 , PhCN, or pyridine as compared to the parent triple-decker compound with a triphenylcorrole macrocycle. The measured $E_{1/2}$ values are linearly related to the number of NO_2Ph groups on the corrole, and the relative magnitude of the shift in potential for each redox reaction was used in conjunction with the results from thin-layer spectro-electrochemistry to assign the initial site of oxidation or reduction on the molecule. The nitrophenyl substituents are also redox-active, and each is reduced to $[\text{C}_6\text{H}_4\text{NO}_2]^-$ in a separate one-electron transfer step at potentials between -1.12 and -1.42 V versus saturated calomel electrode.



INTRODUCTION

The design and synthesis of new sandwich triple-decker tetrapyrrole derivatives represent an important area for researchers interested in exploring the potential use of these compounds in a variety of practical applications, from molecular magnets and nanomaterials to organic thin-film transistors and sensors.^{1–11} The most often studied among the rare earth triple-decker tetrapyrrole derivatives are the homo- and heteroleptic complexes with porphyrin and/or phthalocyanine macrocycles.^{1–11} These compounds can have different substituents at the peripheral positions of the molecular framework of each macrocycle, and a judicious selection of the placement and properties of the substituents enables tuning of the optical, electrical, and electrochemical properties.^{12–17} Tuning the optical and electrochemical properties of triple-decker compounds with porphyrins, phthalocyanines, and related molecules can also be accomplished by varying (i) the type of coordinated metal ions,^{18–23} (ii) the arrangement of the tetrapyrrole macrocycles in the compound,^{24–34} and/or (iii) the nature of the tetrapyrrole macrocycles themselves.^{35–38}

With respect to the latter two points, we recently demonstrated that a corrole macrocycle could be incorporated into triple-decker complexes.^{36,39,40} The properties of corroles differ from those of both porphyrins and phthalocyanines in that these macrocycles are dianionic ligands, while corroles are

trianionic ligands having three inner core amine protons within a contracted tetrapyrrolic ring.⁴¹ Corroles undergo a facile ligand-to-metal electron transfer, introducing so-called “non-innocent” behavior,^{42–46} and can also stabilize the central metal ion of the complex in a formally higher oxidation state than for the related porphyrins or phthalocyanines.^{47,48} These properties of corroles are particularly appealing for investigated applications of the compounds in the fields of catalysis, chemical sensors, and/or dye-sensitized solar cells.^{49–52}

In sharp contrast with the large amount of current research activity involving transition metal corroles,^{49–54} very little is known about the corresponding rare earth complexes with this macrocyclic ligand. To the best of our knowledge, studies of corroles with rare earth metal ions are limited to the monometallic derivatives $(\text{Mes}_2(p\text{-OMePh})\text{Cor})\text{M}$ ($\text{M} = \text{La}$, 4.5DME, Tb, 4DME, or Gd-TACNMe₃)⁵⁵ and triple-decker complexes $\text{M}_2[\text{Pc}(\text{OC}_4\text{H}_9)_8]_2[\text{Cor}(\text{ClPh})_3]$ ($\text{M} = \text{Pr}$ –Tb and Y, except Pm) and $\text{Eu}_2[\text{Pc}(\text{R})_8]_2[\text{Cor}(\text{ClPh})_3]$ ($\text{R} = \text{H}$, OC_5H_{11} , or OC_8H_{17}).^{36,39,40}

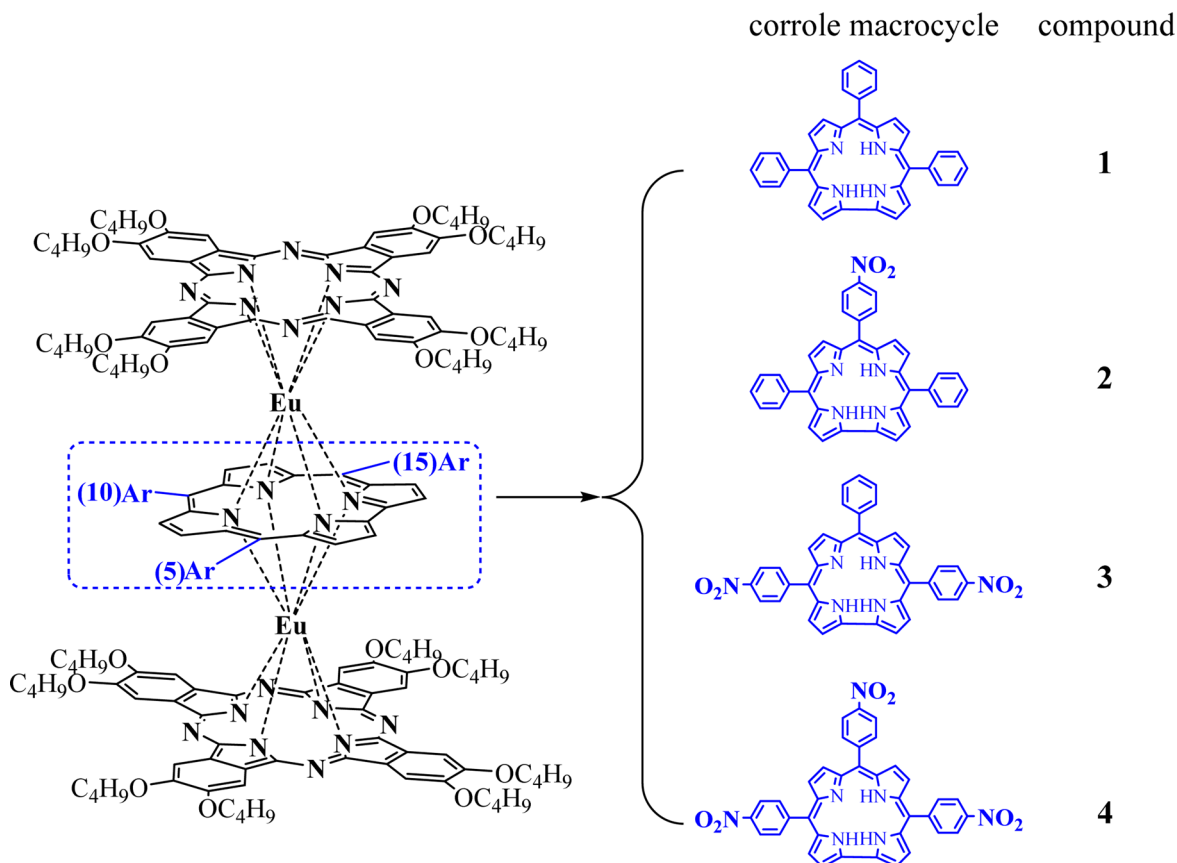
As part of our continued research efforts involving the exploitation and functionalization of triple-decker tetrapyrrole derivatives, we now report the synthesis and characterization of

Received: July 28, 2015

Published: September 11, 2015



Chart 1. Molecular Structures of Investigated Corrole–Phthalocyanine Europium Triple-Decker Complexes



four new heteroleptic corrole–phthalocyanine europium triple-decker complexes containing nitrophenyl substituents on the meso positions of the corrole macrocycle. The investigated compounds are represented as $\text{Eu}_2[\text{Pc}(\text{OC}_4\text{H}_9)_8]_2[\text{Cor}(\text{Ph})_n(\text{NO}_2\text{Ph})_{3-n}]$, where n varies from 0 to 3, $\text{Pc}(\text{OC}_4\text{H}_9)_8$ represents the phthalocyanine macrocycle, and Cor indicates the corrole ligand having NO_2Ph substituents at the 5-meso, 10,15-meso, or 5,10,15-meso positions of the macrocycle (Chart 1). Three different synthetic methods are used for preparing the complexes, two of which are reported here for the first time.

It is known that highly electron-withdrawing character of nitro groups on corrole can be used to direct the orientation of the corrole macrocycle for further functionalization or to facilitate aromatic nucleophilic substitution to form new species.⁴² It has been demonstrated that the presence of one or more nitro groups at the meso- or β -pyrrole positions of a corrole or porphyrin macrocycle will have a large effect on the $E_{1/2}$ for electroreduction of the mononuclear complex, but it was not known what might be observed in the case of the triple-decker species where multiple redox reactions are observed.^{42,56–59} Thus, one aspect of the current study is to understand how nitro substituents introduced at the para-position of the three meso-phenyl rings of the corrole macrocycle in a triple-decker complex will influence the redox potentials in the sandwich corrole–phthalocyanine europium derivatives. This is examined in the present paper where we report electrochemical and spectroscopic characterization of the synthesized triple-decker complexes and use the combined data to assign the probable site of electron transfer.

EXPERIMENTAL SECTION

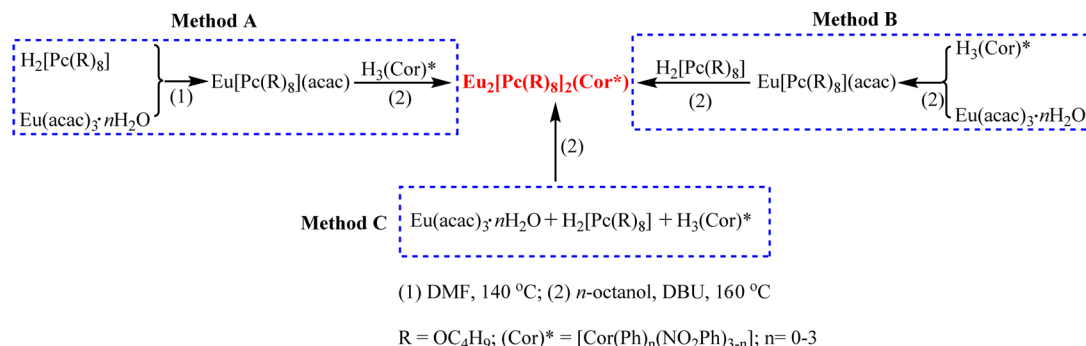
Materials. Reagents and solvents (Sinopharm or Aldrich) were of the highest grade available and were used without further purification, except for *n*-octanol and benzonitrile (PhCN), which was distilled under reduced pressure prior to use from sodium or P_2O_5 , respectively. Tetra-*n*-butylammonium perchlorate (TBAP) from Sigma-Aldrich was used as supporting electrolyte.

Physical Measurements. IR spectra (KBr pellets) were recorded on AVATAR-370 spectrometer. ^1H NMR spectra were recorded in a CDCl_3 solution at 400 MHz using a Bruker Advance 400 spectrometer at 25 °C. Chemical shifts (ppm) were determined with tetramethylsilane as the internal reference. Matrix-assisted laser desorption/ionization time-of-flight (MALDI-TOF) mass spectra were performed on a Bruker BIFLEX III ultrahigh-resolution Fourier transform ion cyclotron resonance (FT-ICR) mass spectrometer with α -cyano-4-hydroxycinnamic acid as matrix. Elemental analyses were performed with FLASH1112A Element Analyzer.

Electrochemistry. Cyclic voltammetry was performed at 298 K using a CHI-730C Electrochemical Workstation. A homemade three-electrode cell was used for cyclic voltammetric measurements and consisted of a glassy carbon working electrode, a platinum counter electrode, and a homemade saturated calomel reference electrode (SCE). The SCE was separated from the bulk of the solution by a fritted glass bridge of low porosity, which contained the solvent/supporting electrolyte mixture. All potentials are referenced to the SCE. High-purity N_2 was used to deoxygenate the solution, and a stream of nitrogen gas was kept over the solution during each electrochemical experiment.

Thin-layer UV–visible (UV–vis) spectro-electrochemical experiments were performed with a home-built thin-layer cell, which has a light transparent platinum net working electrode. Potentials were applied and monitored with an EG&G model 173 potentiostat. Time-resolved UV–vis spectra were recorded with a Hewlett-Packard model 8453 diode array spectrophotometer. High-purity N_2 from trigas was

Scheme 1. Synthesis Routes for Corrole–Phthalocyanine Europium Triple-Decker Complexes



used to deoxygenate the solution and kept over the solution during each electrochemical and spectro-electrochemical experiment.

Synthesis. The free-base phthalocyanine $\text{H}_2[\text{Pc}(\text{OC}_4\text{H}_9)_8]$,⁶⁰ free-base corrole $\text{H}_3[\text{Cor}(\text{Ph})_n(\text{NO}_2\text{Ph})_{3-n}]$,⁵⁸ and $\text{Eu}(\text{acac})_3 \cdot n\text{H}_2\text{O}$ ⁶¹ salt were prepared according to published procedures. The triple-decker complexes were then prepared following three different procedures, two of which differ from each other by the order of adding materials. A summary of the three procedures is given in Scheme 1.

Method A. This method follows the previously published protocol for preparation of triple-decker complexes with mixed phthalocyanine (Pc) and corrole (Cor) macrocycles.^{36,39,40} $\text{Eu}(\text{acac})_3 \cdot n\text{H}_2\text{O}$ (47 mg, ca. 0.1 mmol) was dissolved in dimethylformamide (4 mL); $\text{H}_2[\text{Pc}(\text{OC}_4\text{H}_9)_8]$ (110 mg, 0.1 mmol) was then added, and the resulting solution was heated to 140 °C under a slow stream of nitrogen. After it was heated for 1 h, the solution was cooled to room temperature, and the solvent was evaporated under reduced pressure. During this period the color changed from green to blue, indicating formation of the corresponding monomeric rare earth phthalocyanine complex $\text{Eu}[\text{Pc}(\text{OC}_4\text{H}_9)_8](\text{acac})$. This was then added to $\text{H}_3[\text{Cor}(\text{Ph})_n(\text{NO}_2\text{Ph})_{3-n}]$ (63 mg, 0.1 mmol), which was dissolved in *n*-octanol (4 mL) and heated to 160 °C for 2 h in the presence of 1,8-diazabicyclo[5.4.0]undec-7-ene (DBU) (20 mg, 0.13 mmol) under a slow stream of nitrogen. The resulting green solution was cooled to room temperature, and the volatiles were removed under vacuum. The residue was chromatographed with CHCl_3 as eluent. Small amounts of unreacted $\text{H}_3[\text{Cor}(\text{Ph})_n(\text{NO}_2\text{Ph})_{3-n}]$ and the homoleptic bis-(phthalocyanine) europium complex $\text{Eu}[\text{Pc}(\text{OC}_4\text{H}_9)_8]_2$ were collected as the first and second fractions, respectively. The target mixed-ring triple-decker products were obtained as the third fraction. Repeated chromatography followed by recrystallization from CHCl_3 and CH_3OH gave pure $\text{Eu}_2[\text{Pc}(\text{OC}_4\text{H}_9)_8]_2[\text{Cor}(\text{Ph})_n(\text{NO}_2\text{Ph})_{3-n}]$ as a gray-green solid. The yields for compounds 1–4 by Method A were 54, 40, 47, and 50%, respectively.

Method B. In this method the order of adding reagents to the reaction mixture is reversed as compared to Method A (see Scheme 1). A mixture of $\text{Eu}(\text{acac})_3 \cdot n\text{H}_2\text{O}$ (47 mg, ca. 0.1 mmol) and $\text{H}_3[\text{Cor}(\text{Ph})_n(\text{NO}_2\text{Ph})_{3-n}]$ (63 mg, 0.1 mmol) in *n*-octanol (4 mL) containing DBU (20 mg, 0.13 mmol) was heated at 160 °C under a slow stream of nitrogen. The progress of the reaction was monitored by UV–vis spectroscopy and thin-layer chromatography (TLC). After complete disappearance of the starting material (ca. 1 h), free base phthalocyanine $\text{H}_2[\text{Pc}(\text{OC}_4\text{H}_9)_8]$ (110 mg, 0.1 mmol) was added to the hot solution, and the progress of the reaction was monitored by TLC and UV–vis spectroscopy. After 2 h, the resulting green solution was cooled to room temperature, and the volatiles were removed under vacuum. The subsequent reaction workup was performed as described in Method A. Yields for compounds 1–4 by Method B were 15, 5, 9, and 13%, respectively.

Method C. This is a new method involving a one-pot synthesis. A mixture of $\text{Eu}(\text{acac})_3 \cdot n\text{H}_2\text{O}$ (47 mg, ca. 0.1 mmol), $\text{H}_3[\text{Cor}(\text{Ph})_n(\text{NO}_2\text{Ph})_{3-n}]$ (63 mg, 0.1 mmol), and $\text{H}_2[\text{Pc}(\text{OC}_4\text{H}_9)_8]$ (110 mg, 0.1 mmol) in *n*-octanol (4 mL) containing DBU (20 mg, 0.13 mmol) was heated at 160 °C for 3–5 h under a slow stream of nitrogen to give a dark green solution. The solvent was removed under

vacuum. The subsequent reaction workup was performed as described in Method A. Yields for compounds 1–4 by the one-pot synthetic method were 43, 31, 36, and 40%, respectively.

$\text{Eu}_2[\text{Pc}(\text{OC}_4\text{H}_9)_8]_2[\text{Cor}(\text{Ph})_3]$ (1). ¹H NMR (400 MHz, CDCl_3): δ 5.35 (s, 16 H, OCH_2), 4.88 (s, 16 H, OCH_2), 2.53 (t, 32 H, CH_2), 2.16 (m, 32 H, CH_2), 1.49 (t, 48 H, CH_3); MALDI-TOF mass: Calcd 3006.272, Found 3007.689. Anal. Calcd (%) for $\text{Eu}_2\text{C}_{165}\text{H}_{183}\text{N}_{20}\text{O}_{16}$: C 65.92, H 6.13, N 9.32; found: C 65.64, H 5.91, N 9.32. Main IR band (cm^{-1}): 1311 (w), 1380 (s).

$\text{Eu}_2[\text{Pc}(\text{OC}_4\text{H}_9)_8]_2[\text{Cor}(\text{Ph})_2(\text{NO}_2\text{Ph})]$ (2). ¹H NMR (400 MHz, CDCl_3): δ 5.33 (s, 16 H, OCH_2), 4.84 (s, 16 H, OCH_2), 2.51 (t, 32 H, CH_2), 2.14 (m, 32 H, CH_2), 1.47 (t, 48 H, CH_3); MALDI-TOF mass: Calcd 3051.269, Found 3052.650. Anal. Calcd (%) for $\text{Eu}_2\text{C}_{165}\text{H}_{182}\text{N}_{21}\text{O}_{18}$, (1/2 CHCl_3): C 63.90, H 5.91, N 9.46; found: C 64.02, H 5.94, N 9.81. Main IR band (cm^{-1}): 1311 (w), 1380 (s), 1340 (m).

$\text{Eu}_2[\text{Pc}(\text{OC}_4\text{H}_9)_8]_2[\text{Cor}(\text{Ph})(\text{NO}_2\text{Ph})_2]$ (3). ¹H NMR (400 MHz, CDCl_3): δ 5.57 (s, 16 H, OCH_2), 5.10 (s, 16 H, OCH_2), 2.56 (t, 32 H, CH_2), 2.18 (m, 32 H, CH_2), 1.50 (t, 48 H, CH_3), −2.39 (b, 1H, H); MALDI-TOF mass: Calcd 3096.267, Found 3097.452. Anal. Calcd (%) for $\text{Eu}_2\text{C}_{165}\text{H}_{181}\text{N}_{22}\text{O}_{20}$, (1/2 CHCl_3): C 62.98, H 5.80, N 9.76; found: C 62.89, H 5.90, N 10.08. Main IR band (cm^{-1}): 1311 (w), 1380 (s), 1340 (m).

$\text{Eu}_2[\text{Pc}(\text{OC}_4\text{H}_9)_8]_2[\text{Cor}(\text{NO}_2\text{Ph})_3]$ (4). ¹H NMR (400 MHz, CDCl_3): δ 5.55 (s, 16 H, OCH_2), 5.02 (s, 16 H, OCH_2), 2.53 (t, 32 H, CH_2), 2.16 (m, 32 H, CH_2), 1.46 (t, 48 H, CH_3); MALDI-TOF mass: Calcd 3141.264, Found 3142.940. Anal. Calcd (%) for $\text{Eu}_2\text{C}_{165}\text{H}_{180}\text{N}_{23}\text{O}_{22}$, (1/2 CHCl_3): C 62.10, H 5.68, N 10.06; found: C 61.67, H 5.56, N 10.01. Main IR band (cm^{-1}): 1311 (w), 1380 (s), 1339 (m).

Crystal Data for $\text{Eu}_2[\text{Pc}(\text{OC}_4\text{H}_9)_8]_2[\text{Cor}(\text{Ph})(\text{NO}_2\text{Ph})_2]$ 3. Single-crystal data were collected on a Rigaku Saturn 724+ CCD X-ray diffractometer by using monochromated Mo $K\alpha$ radiation ($\lambda = 0.71070 \text{ \AA}$) at 120 K. Final unit cell parameters were derived by global refinements and reflections obtained from integration of all the frame data. The collected frames were integrated by using the preliminary cell-orientation matrix. CrysAlisPro Agilent Technologies software was used for collecting frames of data, indexing reflections, and determination of lattice constants; CrysAlisPro Agilent Technologies software was also used for integrating the intensity of reflections and scaling; SCALE3 ABSPACK was used for absorption correction. The structures were solved by the direct method (SHELXS-97) and refined by full-matrix least-squares (SHELXL-97) on F^2 .⁶⁵ Anisotropic thermal parameters were used for the nonhydrogen atoms, and isotropic parameters were used for the hydrogen atoms. Hydrogen atoms were added geometrically and refined using a riding model. Crystal data: $\text{Eu}_2\text{C}_{166}\text{H}_{189}\text{N}_{22}\text{O}_{23}$, $M_r = 699.46 \text{ g mol}^{-1}$, monoclinic, space group $P2_1/c$, $a = 28.870(6) \text{ \AA}$, $b = 23.020(5) \text{ \AA}$, $c = 24.010(5) \text{ \AA}$, $\alpha = 90.00^\circ$, $\beta = 102.65(3)^\circ$, $\gamma = 90.00^\circ$, $V = 15569(65) \text{ \AA}^3$, $Z = 4$, $F(000) = 6576$, $\mu = 0.874 \text{ mm}^{-1}$, $T = 100 \text{ K}$, $\theta_{\min} = 3.0^\circ$, $\theta_{\max} = 26.0^\circ$, 1937 parameters, 0 restraints, $R_1[I > 2\sigma] = 0.1198$, $R_2[I > 2\sigma] = 0.2864$, $R_{\text{int}} = 0.1269$, $R_{\text{w}} = 0.2935$, $S = 1.138$. ($R_1 = \sum |F_o| - |F_c| / \sum |F_o|$, $R_{\text{w}} = [\sum w(F_o^2 - F_c^2)^2 / \sum w(F_o^2)^2]^{1/2}$). Additional crystallographic information is available in the Supporting Information.

RESULTS AND DISCUSSION

Synthesis and Characterization. In comparison to the well-established synthetic routes used for preparing rare earth porphyrin and/or phthalocyanine triple-decker complexes,^{1–4,6} the field of rare earth corrole–phthalocyanine heteroleptic complexes is still in its infancy, and only one synthetic method has been reported as recently described by our group.^{36,39,40} With this in mind, we wished to investigate further the scope of the published synthetic method and to also explore modifications that might enrich the synthetic yield and also simplify the experimental procedures. This is addressed in the current paper where we have described three methods for obtaining a new series of nitrophenyl corrole–phthalocyanine europium triple-decker complexes.

According to the earlier reported method (Scheme 1, Method A), synthesis of $\text{Eu}_2[\text{Pc}(\text{OC}_4\text{H}_9)_8]_2[\text{Cor}(\text{Ph})_n(\text{NO}_2\text{Ph})_{3-n}]$, where $n = 0–3$, afforded the sandwich triple-decker complexes in 40–54% yield. We then modified the initially reported protocol in Method A by using the free base corrole as starting material with the aim of avoiding replacement of solvent, as shown in Scheme 1, Method B. In Method B, the target complexes 1–4 were obtained by prior generation of the “half-sandwich” corrole complex $\text{Eu}[\text{Cor}(\text{Ph})_n(\text{NO}_2\text{Ph})_{3-n}]$ from $\text{H}_3[\text{Cor}(\text{Ph})_n(\text{NO}_2\text{Ph})_{3-n}]$ and $\text{Eu}(\text{acac})_3 \cdot n\text{H}_2\text{O}$ in *n*-octanol containing 1,8-diazabicyclo[5.4.0]undec-7-ene (DBU) at 170 °C, followed by treatment with the free-base phthalocyanine. The reaction between $\text{H}_3[\text{Cor}(\text{Ph})_n(\text{NO}_2\text{Ph})_{3-n}]$ and $\text{Eu}(\text{acac})_3 \cdot n\text{H}_2\text{O}$ also proceeded rapidly, and in 1 h a complete disappearance of the starting compounds was confirmed by TLC analysis, while also monitoring the progress of the reaction mixture by UV–vis spectroscopy. The UV spectrum of the product formed prior to addition of $\text{H}_2[\text{Pc}(\text{OC}_4\text{H}_9)_8]$ showed the typical spectral features of a metal corrole, presumably the “half-sandwich” corrole complex $\text{Eu}[\text{Cor}(\text{Ph})_n(\text{NO}_2\text{Ph})_{3-n}]$. Note that attempts to isolate $\text{Eu}[\text{Cor}(\text{Ph})_n(\text{NO}_2\text{Ph})_{3-n}]$ were not successful because of rapid decomposition during chromatography, giving the free base corrole as a product. Compared with Method A, the procedures of Method B were simple, but the yield was lower (5–15%), due to the presence of unreacted free base phthalocyanine as a third fraction, while the target triple-decker complex was the fourth fraction in the separation. Thus, this method was not successful in that it did not improve the yield.

However, we did find that the stepwise reaction procedures of Methods A and B could be simplified to a “one-step” procedure (Scheme 1, Method C). In this method, treatment of $\text{Eu}(\text{acac})_3 \cdot n\text{H}_2\text{O}$ with $\text{H}_3[\text{Cor}(\text{Ph})_n(\text{NO}_2\text{Ph})_{3-n}]$ and $\text{H}_2[\text{Pc}(\text{OC}_4\text{H}_9)_8]$ in the presence of DBU in *n*-octanol led to formation of the corresponding $\text{Eu}_2[\text{Pc}(\text{OC}_4\text{H}_9)_8]_2[\text{Cor}(\text{Ph})_n(\text{NO}_2\text{Ph})_{3-n}]$, where $n = 0–3$. Although chromatographic purification afforded trace quantities of the free base phthalocyanine as the third fraction, the reaction yields (31–43%), calculated with respect to the starting material free base phthalocyanine, are comparable with yields obtained from the published protocol, Method A.

In addition to elemental analysis, the four synthesized triple-decker compounds were characterized by various methods. Mass spectrometry is a powerful technique for characterizing this class of compounds as some of the lanthanides give very distinct isotopic patterns. The MALDI-TOF mass spectra of the four compounds showed intense signals for the molecular ion $[\text{M} + \text{H}]^+$ (Figure S1), providing strong evidence for the

identity of the compounds. Because of the presence of an unpaired electron and the paramagnetic nature of the europium ions, satisfactory ^1H NMR data for these sandwich complexes could not be obtained. However, the complexes all exhibited an intense IR band at 1380 cm^{-1} and an extremely weak band at ca. 1311 cm^{-1} , suggesting the dianionic nature of the two phthalocyanine ligands in the mixed triple-decker complexes (Figure S2). A medium-intensity IR band is also seen for compounds 2–4 at $1339–1340\text{ cm}^{-1}$ and is assigned to the N–O stretching vibrations of NO_2 on the NO_2Ph substituents (Figure S2).

Crystals of 3 suitable for X-ray characterization were grown by slow diffusion of methanol into a concentrated chloroform solution, thereby allowing for elucidation of the structure, which is illustrated in Figure 1. Compound 3 crystallizes in the

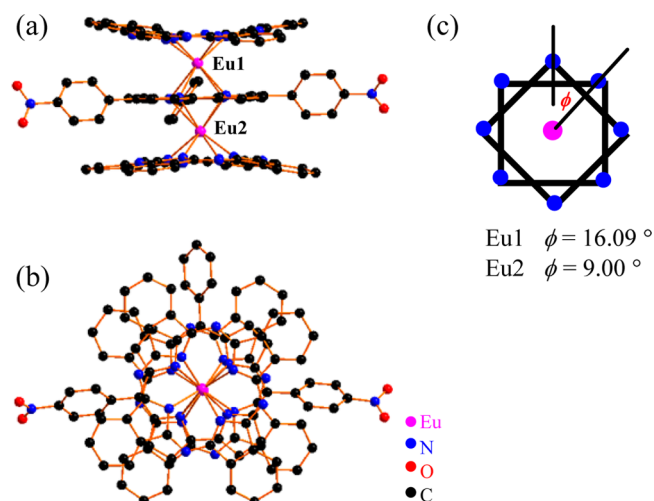


Figure 1. Molecular structure of $\text{Eu}_2[\text{Pc}(\text{OC}_4\text{H}_9)_8]_2[\text{Cor}(\text{Ph})(\text{NO}_2\text{Ph})_2]$ 3 showing (a) side view, (b) top view, with all the hydrogen atoms, OC_4H_9 substituents on the phthalocyanine rings, and solvent molecules omitted for clarity, and (c) twist angles around Eu metal ions.

monoclinic system with a $P2_1/c$ space group, which is different from what was earlier reported for $\text{Eu}_2[\text{Pc}(\text{OC}_8\text{H}_{17})_8]_2[\text{Cor}(\text{ClPh})_3]$ ³⁶ and $\text{Eu}_2[\text{Pc}(\text{OC}_4\text{H}_9)_8]_2[\text{Cor}(\text{ClPh})_3]$,³⁹ both of which are in the triclinic system with a $P\bar{1}$ space group. Each cell for compound 3 contains four sandwich triple-decker molecules, four methanol molecules, and eight water molecules. The mixed tetrapyrrole nature of the compounds is unambiguously revealed in Figure 1, which has the hydrogen atoms, OC_4H_9 substituents on the phthalocyanine rings, and solvent molecules omitted for clarity. The two outer phthalocyanine ligands are connected by two europium ions sharing a common corrole ligand, forming the heteroleptic triple-decker complex. Each europium ion is octa-coordinated by the isoindole and pyrrole nitrogen atoms of the outer Pc ring and the central Cor ring, and both exhibit slightly distorted square prism coordination geometries with a twist angle ϕ of 16.09° for Eu1 and 9.00° for Eu2 (Figure 1c). Selected bond distances and angles are given in Table S1. As also occurs in earlier characterized triple-decker tetrapyrrole complexes with mixed Pc and Cor macrocycles, the two europium ions are not equidistant from the coordinated Pc and Cor rings,^{36,39} but rather lie closer to the Pc rings than to the plane of the Cor ligand (1.349 vs 1.791 \AA for Eu1 and 1.406 vs 1.786 \AA for Eu2).

Table 1. Electronic Absorption Data for $\text{Eu}_2[\text{Pc}(\text{OC}_4\text{H}_9)_8]_2[\text{Cor}(\text{Ph})_n(\text{NO}_2\text{Ph})_{3-n}]$ in CH_2Cl_2 , PhCN, and Pyridine

solvent	no. of NO_2 groups, n	λ_{max} , nm (log ϵ)				
CH_2Cl_2	0	294 (5.17)	351 (5.27)	420 (4.90)	534 (4.57) ^a	682 (4.79)
	1	294 (5.28)	351 (5.36)	425 (4.97)	542 (4.66) ^a	674 (4.93)
	2	294 (5.19)	352 (5.27)	433 (4.90)	545 (4.58) ^a	685 (4.88)
	3	294 (5.17)	351 (5.24)	436 (4.87)	547 (4.56) ^a	680 (4.86)
PhCN	0	<i>b</i>	353 (5.06)	421 (4.71)	530 (4.33) ^a	680 (4.65)
	1	<i>b</i>	353 (5.18)	430 (4.80)	544 (4.47) ^a	675 (4.79)
	2	<i>b</i>	354 (5.24)	435 (4.86)	545 (4.53) ^a	683 (4.90)
	3	<i>b</i>	353 (5.07)	439 (4.70)	550 (4.39) ^a	680 (4.73)
Py	0	<i>b</i>	353 (5.25)	420 (4.92)	534 (4.52) ^a	680 (4.82)
	1	<i>b</i>	354 (5.23)	429 (4.84)	542 (4.47) ^a	672 (4.82)
	2	<i>b</i>	354 (5.27)	433 (4.92)	545 (4.55) ^a	684 (4.93)
	3	<i>b</i>	353 (5.28)	437 (4.90)	547 (4.55) ^a	680 (4.95)

^aBroad and weak band. ^bThis band could not be observed in PhCN or pyridine.

Table 2. Half-Wave Potentials ($E_{1/2}$, V vs SCE) and Proposed Sites of Electron Transfer (Cor or Pc) for the Oxidations and Reductions of $\text{Eu}_2[\text{Pc}(\text{OC}_4\text{H}_9)_8]_2[\text{Cor}(\text{Ph})_n(\text{NO}_2\text{Ph})_{3-n}]$ (1–4) and $\text{Eu}_2[\text{Pc}(\text{OC}_4\text{H}_9)_8]_2[\text{Cor}(\text{PhCl})_3]$ (5) in PhCN, CH_2Cl_2 , or Pyridine Containing 0.1 M TBAP

solvent	no. of NO_2 , n	cpd	oxidation					reduction				
			fifth (Cor)	fourth	third (Pc)	second (Pc)	first (Cor)	first (Cor)	second (NO_2Ph)	third (NO_2Ph)	fourth	fifth
CH_2Cl_2	0	1	1.41	1.28	1.07	0.69	0.29	−0.16			−1.36	−1.58
	1	2	1.48	1.30	1.08	0.71	0.33	−0.08	−1.40 ^a		−1.55 ^a	−1.76 ^a
	2	3	1.54	1.33	1.09	0.75	0.37	0.00	−1.28 ^a	−1.42 ^a	−1.58 ^a	−1.81 ^a
	3	4	1.60	1.37	1.10	0.76	0.41	0.07	−1.26 ^a	−1.41 ^a	−1.63 ^a	−1.86 ^a
		5 ^b	1.46	1.30	1.09	0.72	0.33	−0.11			−1.36	−1.58
PhCN	0	1	1.43	1.31	1.06	0.68	0.29	−0.07			−1.29	−1.45
	1	2	1.48	1.33	1.07	0.70	0.32	−0.03	−1.27		−1.44	−1.66 ^a
	2	3	1.52	1.36	1.09	0.71	0.35	0.02	−1.21	−1.33	−1.46	−1.70 ^a
	3	4	1.59	1.41	1.11	0.74	0.38	0.08	−1.19	−1.32	−1.50	−1.80 ^a
		5	1.43	1.31	1.08	0.71	0.33	−0.04			−1.25	−1.44
pyridine	0	1				0.72	0.34	−0.05			−1.25	−1.47
	1	2				0.75	0.38	0.02	−1.21		−1.36	−1.51
	2	3				0.79	0.42	0.07	−1.14	−1.29	−1.41	−1.57
	3	4				0.82	0.46	0.12	−1.12	−1.29	−1.46	−1.66
		5				0.75	0.38	0.00			−1.24	−1.44

^aIrreversible peak potential, E_p , at scan rate of 0.10 V/s. ^bData for compound 5 is taken from ref 39.

The Eu1-Eu2 separation is 3.578 Å, which is slightly longer than that in $\text{Eu}_2[\text{Pc}(\text{OC}_4\text{H}_9)_8]_2[\text{Cor}(\text{ClPh})_3]$ (3.586 Å),³⁶ probably because of a steric effect of the NO_2 groups. Interestingly, the Eu-N distances are also not equivalent for the two metal ions. The average $\text{Eu1-N}[\text{Pc}(\text{OC}_4\text{H}_9)_8]$ bond length (2.386 Å) is significantly shorter than the average $\text{Eu1-N}[\text{Cor}(\text{Ph})(\text{NO}_2\text{Ph})_2]$ bond length (2.594 Å), and the $\text{Eu2-N}[\text{Pc}(\text{OC}_4\text{H}_9)_8]$ (2.424 Å) distance is also shorter than the $\text{Eu2-N}[\text{Cor}(\text{Ph})(\text{NO}_2\text{Ph})_2]$ distance (2.590 Å). These structural features are similar to what was earlier reported for $\text{Eu}_2[\text{Pc}(\text{OC}_8\text{H}_{17})_8]_2[\text{Cor}(\text{ClPh})_3]$ ³⁶ and $\text{Eu}_2[\text{Pc}(\text{OC}_4\text{H}_9)_8]_2[\text{Cor}(\text{ClPh})_3]$ ³⁹ but clearly different from other tetrapyrrole rare earth triple-decker complexes, such as $\text{Er}_2(\text{Pc})_2[\text{Pc}(\text{OC}_8\text{H}_{17})_8]$,⁶² $\text{Ce}_2[\text{Pc}(\text{OMe})_8][(\text{TPP})_2]$,⁶³ and $\text{Nd}_2(\text{Nc})[(\text{OEP})_2]$,⁶⁴ which are centrosymmetric, with two identical metal environments. This could be attributed to the different crystal packing forces for these complexes.

Electronic Absorption Spectra. The electronic absorption spectra of the currently investigated triple-decker complexes were recorded in CH_2Cl_2 , PhCN, and Py, and the data are summarized in Table 1. As seen in the Table, a characteristic phthalocyanine N band for compounds 1–4 is

clearly observed at 294 nm in CH_2Cl_2 . This band is assigned to electronic transitions associated with the deeply filled orbitals and the LUMO⁶⁵ and could not be detected in PhCN or Py due to the limited UV–visible spectral window of these solvents. Two sharp bands of 1–4 are located at 351–354 and 420–437 nm in CH_2Cl_2 , PhCN, or Py, and these are attributed to the Soret bands of the complexes having a predominant phthalocyanine and corrole character, respectively. Two Q bands are also seen at 534–547 nm and 672–685 nm. These values are similar to bands for the analogous complexes of $\text{M}_2[\text{Pc}(\text{OC}_4\text{H}_9)_8]_2[\text{Cor}(\text{ClPh})_3]$ ($\text{M} = \text{Pr-Tb}$ and Y , except Pm) and $\text{Eu}_2[\text{Pc}(\text{R})_8]_2[\text{Cor}(\text{ClPh})_3]$ ($\text{R} = \text{H}$, OC_5H_{11} , or OC_8H_{17}).^{36,39,40} An intense Q-band at ~680 nm is also observed for double- or triple-decker phthalocyanine complexes,^{66,67} and, on this basis, the bands at 672–685 nm for the currently investigated compounds are also assigned to bands of the Pc macrocycles.

As shown in Table 1, three of the five UV–visible bands of the investigated complexes are sensitive to substituents on the corrole macrocycle, while two of the absorption bands are virtually independent of the corrole ring substituents. As will be demonstrated in the spectro-electrochemistry section of the

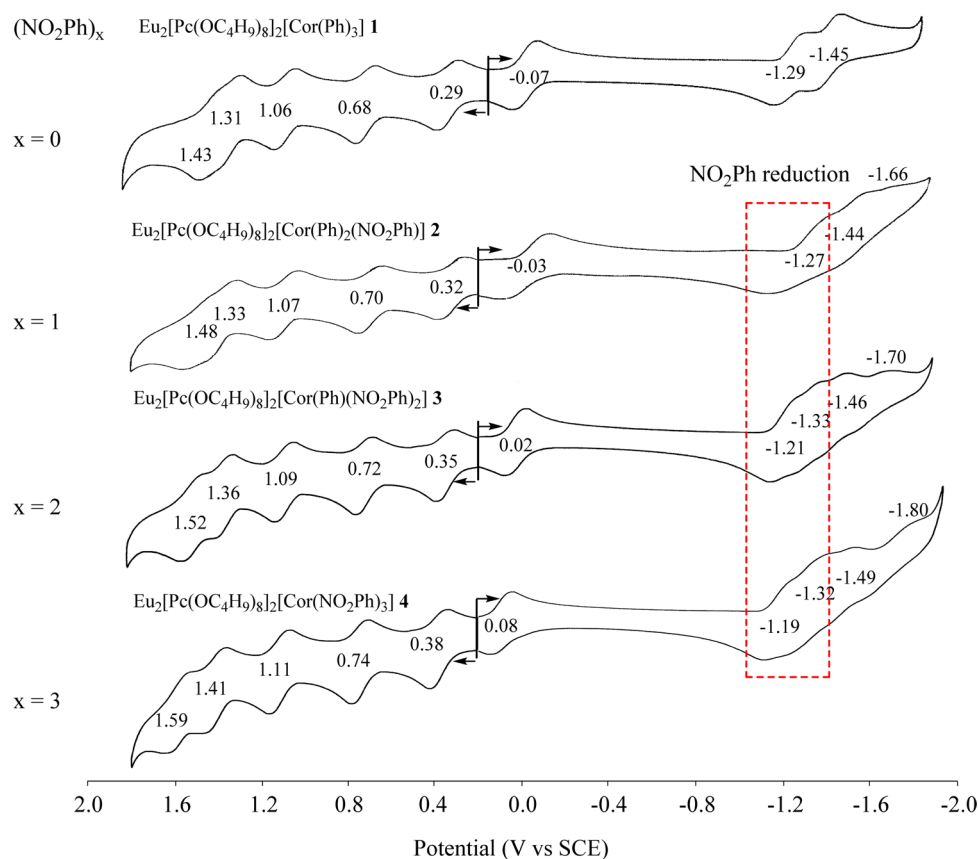


Figure 2. Cyclic voltammograms of compounds **1–4** in PhCN containing 0.1 M TBAP. Reductions of the *meso*-NO₂Ph substituents are indicated by processes within the boxed area.

manuscript, the changes in intensity or position of the 420–439 nm (corrole) band and 672–684 nm (phthalocyanine) bands after oxidation or reduction can be used to provide indirect evidence for the site of electron transfer being predominantly corrole or phthalocyanine-centered in a specific redox process.

The near-IR electronic absorption spectra of compounds **1–4** were also measured in CH₂Cl₂, and an example of the spectrum is given in Figure S3 for compound **1**. The presence of the weak and broad band from 1300 to 2300 nm suggests a neutral radical nature of the investigated triple-decker complexes.³⁹

Electrochemistry. Corrole–phthalocyanine rare earth triple-decker complexes in CH₂Cl₂ containing 0.1 M TBAP were recently reported to undergo up to eight reversible or quasireversible one-electron oxidations and reductions, all of which are attributed to the successive removal or addition of electrons from the ligand-based orbitals of the compound.^{36,39} The addition of 1–3 nitrophenyl groups at the *meso* positions of the corrole macrocycle in compounds **2–4** should lead to additional reactions being observed at the redox active NO₂Ph substituents^{56,57} as well as to a progressive shift of all redox potentials toward more positive values (easier reductions and harder oxidations) as compared to the parent triple-decker compound **1** with a central triphenylcorrole ligand. However, it was not clear what would be the magnitude of the potential shift for each added electron-withdrawing NO₂ group, since this would depend upon the specific site of each electron transfer. It was also not clear if the nitrobenzene substituents on compounds **3** and **4** would interact with each other and be reduced at different half-wave potentials as occurs for some

monomacrocyclic corroles with these substituents,⁵⁷ or if the redox-active NO₂Ph substituents would be non-interacting and all be reduced at the same half-wave potential as has been reported to occur for other corroles with *meso*-NO₂Ph groups.^{57,58}

To answer these questions, the four Eu₂[Pc(OC₄H₉)₈]₂–[Cor(Ph)_{*n*}(NO₂Ph)_{3–*n*}] complexes containing different numbers of NO₂Ph groups were examined as to their electrochemistry in three nonaqueous solvents (CH₂Cl₂, PhCN, and Py) containing 0.1 M TBAP. A summary of the measured half-wave potentials in the different solvents is given in Table 2, which includes the proposed site of the initial electron transfer based on analysis of the electrochemical and spectroscopic data. Examples of cyclic voltammograms in the three solvents are shown in Figure 2 (PhCN), Figure S4 (CH₂Cl₂), and Figure S5 (Py).

Compound **1**, which has no nitro substituents on the corrole (see Chart 1), exhibits five oxidations and three reductions in PhCN (Figure 2) or CH₂Cl₂ (Figure S4), both containing 0.1 M TBAP. Each redox reaction involves a reversible one-electron transfer, and each is attributed to a ligand-based redox process. Similar current–voltage curves are observed for reduction of compound **1** in Py (Figure S5), but only two oxidations can be detected in this solvent due to the limited positive potential window of ~1.0 V.

As expected, the electron-withdrawing nitrophenyl groups on the corrole macrocycles of **2**, **3**, and **4** induce a positive shift of all oxidations as compared to the parent compound **1**, which lacks NO₂ substituents. For example, as seen in Figure 2, the reversible *E*_{1/2} value for the first oxidation of **1** (with no NO₂

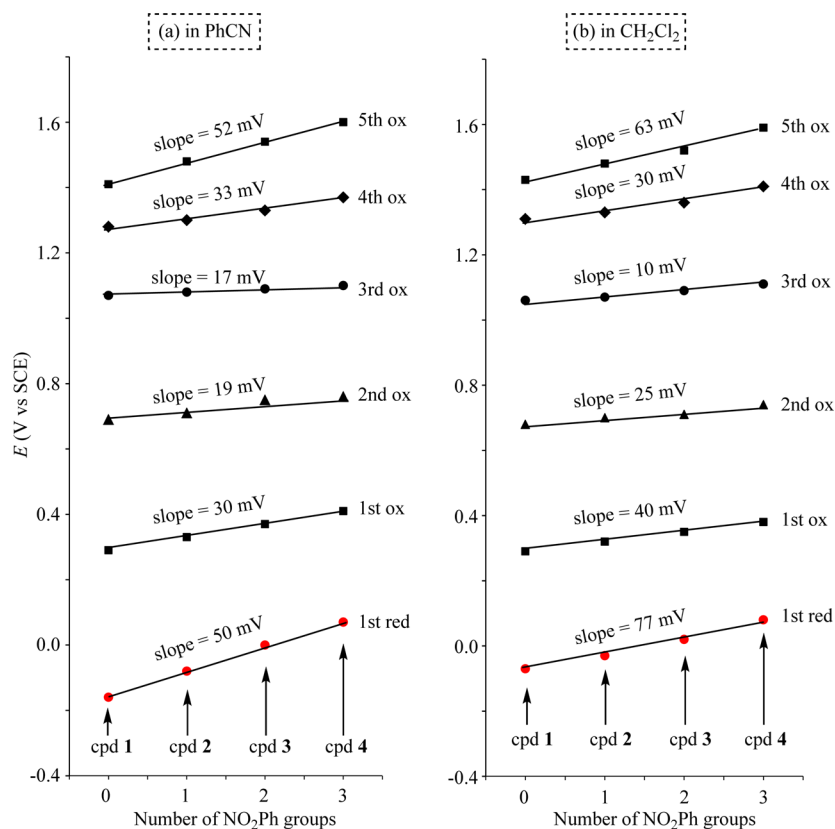


Figure 3. Plots of redox potentials vs the number of NO₂Ph groups on compounds 1–4 in (a) PhCN and (b) CH₂Cl₂ containing 0.1 M TBAP.

groups) is located at 0.29 V, while $E_{1/2}$ for the same redox reaction shifts to 0.32 V for 2 (which contains one NO₂ group), 0.35 V for 3 (with two NO₂ groups), and 0.38 V for 4 (with three NO₂ groups). The difference in $E_{1/2}$ values between the reversible one-electron oxidations of 1 and 4 is 90 mV in PhCN (Figures 2), 120 mV in CH₂Cl₂ (Figures S4), and 170 mV in Py (Figures S5).

A significant positive shift in $E_{1/2}$ also occurs for the first ligand-based reduction of compounds 2–4 as compared to compound 1 under the same solution conditions. This is seen from the electrochemical data in Table 2 as well as from the cyclic voltammograms in Figure 2 (PhCN), Figure S4 (CH₂Cl₂), and Figure S5 (py). The $E_{1/2}$ values for the first one-electron reduction of compounds 1–4 in PhCN are located at –0.07, –0.03, 0.02, and 0.08 V, respectively, and the difference in $E_{1/2}$ between compounds 1 and 4 is 150 mV. This $\Delta E_{1/2}$ value increases to 170 mV in pyridine (Figure S5) and to 230 mV in CH₂Cl₂ (Figure S4), indicating that the potentials for reduction are dependent not only upon the electron-withdrawing characteristics of the *meso*-nitrophenyl substituents but also upon the solvent.

Smaller positive shifts in potential with increase in the number of NO₂ groups are seen for the second, third, and fourth oxidations of 1–4 in PhCN, and the same trend in $E_{1/2}$ with the number of NO₂Ph groups on the compound occurs in CH₂Cl₂ and py as shown in Figures 2, S4, and S5, as well as in Table 2.

Compound 1 (which has no NO₂ groups) exhibits three reversible one-electron transfer steps in PhCN containing 0.1 M TBAP. The first reduction is at $E_{1/2}$ = –0.07 V, the second at $E_{1/2}$ = –1.29 V, and the third at $E_{1/2}$ = –1.45 V (Figure 2). In contrast, four reductions can be seen in the cyclic voltammo-

gram of 2 in PhCN (which has one NO₂ group). These reductions are located at $E_{1/2}$ = –0.03, –1.27, –1.44, and E_{pc} = –1.66 V, respectively (Figure 2). The second reduction of 2 is assigned to the *meso*-NO₂Ph substituent and the $E_{1/2}$ of –1.27 V in PhCN and is shifted negatively by 80 mV as compared to the $E_{1/2}$ of –1.19 V for reduction of unlinked nitrobenzene under the same solution condition (Figure S6). The second reduction of compounds 3 and 4 is also assigned as a one-electron addition to a *meso*-NO₂Ph group on the macrocycle. This conversion of the linked NO₂Ph group to [NO₂Ph][–] occurs at $E_{1/2}$ = –1.21 and –1.19 V for 3 and 4, respectively, the latter value being exactly the same as the half-wave potential for reduction of unlinked nitrobenzene in PhCN (see Figure S6).

The singly reduced [NO₂Ph][–] product of the *meso*-nitrobenzene substituents on compounds 2, 3, and 4 is unstable in CH₂Cl₂ containing trace water or protons, and this leads to irreversible processes as seen in Figure S4. However, greater reversibility is obtained in PhCN and pyridine where reversible half-wave potentials for the stepwise reduction of each NO₂Ph group can be measured from voltammograms of the types shown in Figures 2, S5, and S7. For example, compound 3 exhibits five one-electron reductions in pyridine ($E_{1/2}$ = 0.07, –1.14, –1.29, –1.41, and –1.57 V), the second and third of which correspond to electron addition at the 5 and 15 *meso*-NO₂Ph groups on the compound (Figures S7). The fact that the two equivalent NO₂Ph groups in compound 3 are reduced at different half-wave potentials indicates an interaction between these redox-active centers across the molecule. The $\Delta E_{1/2}$ of 150 mV between these two one-electron reductions of the NO₂Ph groups in pyridine (and 120 mV in PhCN) indicates a moderately strong interaction. Moreover, reduction

of the three *meso*-NO₂Ph substituents on compound **4** in pyridine occurs in two steps, the first of which involves a reversible one-electron addition at $E_{1/2} = -1.12$ V; the second involves two overlapping one-electron transfer steps at the same half-wave potential of -1.29 V (Figure S5). Again, the first one-electron reduction potential of the *meso*-NO₂Ph groups on compounds **3** and **4** are virtually identical to each other in pyridine (-1.12 and -1.14 V), and they are also almost identical to the $E_{1/2}$ for reduction of unlinked nitrobenzene under the same solution conditions ($E_{1/2} = -1.15$ V, as illustrated in Figure S6).

In summary, compounds **2–4** exhibit one or two more reductions than compound **1** as shown in Figures 2, S4, and S5. These reductions are assigned to the electroactive NO₂Ph groups, each of which is reversibly converted to its [NO₂Ph][−] form in a stepwise one-electron transfer. This result is quite different from what was reported for reduction of the *meso*-NO₂Ph groups on copper and cobalt corroles, where all three nitrobenzene reductions occur at the same half-wave potential,⁵⁸ and it is also different from free-base, palladium, or zinc porphyrins having nitrophenyl substituents at the four *meso* positions of the macrocycle, where a single multielectron reduction is observed.⁵⁹

Finally, note that the reduction of unlinked nitrobenzene in CH₂Cl₂ containing 0.1 M TBAP proceeds in two steps, the second of which is irreversible and located at a peak potential of ca. -2.0 V (Figure S6c). Similar irreversible reductions are seen for the compounds **2–4** in CH₂Cl₂ (Figure S4), but the exact potential of these electron transfers could not be easily measured, nor could the site of electron transfer be precisely determined.

As will be shown in the following section, the measured $E_{1/2}$ values for oxidation of **1–4** are linearly related to the number of NO₂Ph groups on the corrole, with the magnitude of the shift in potential for each redox reaction being related to the predominant macrocyclic site of electron transfer, either corrole or phthalocyanine.

Substituent Effects, Spectroelectrochemistry, and Site of Electron Transfer. As described above, and shown in Figure 2, half-wave potentials for the five oxidations and first reduction of compounds **1–4** vary with the number of electron-withdrawing NO₂Ph groups on the compounds. Increasing the number of NO₂Ph groups on the corrole leads to a progressive positive shift in the reversible half-wave potentials for the first one-electron reduction and five one-electron oxidations of the compounds, with the magnitude of the shift being dependent upon both the solvent and the specific redox reaction as shown by the plots in Figure 3. A linear correlation exists between $E_{1/2}$ and the number of NO₂Ph groups on the corrole for the six examined redox reactions in PhCN or CH₂Cl₂, and the trend in the substituent effect is the same in both solvents, namely, a much larger effect of the NO₂Ph groups on $E_{1/2}$ for the first reduction and first oxidation, where the slopes of the plots in PhCN (Figure 3a) are 50 and 30 mV as compared to the second and third oxidations of the same compounds in PhCN where the slopes are 19 and 17 mV, respectively. The same relative trend in substituent effects is seen in CH₂Cl₂ (Figure 3b), where the largest slope is seen for the first reduction (77 mV), and the smallest is seen for the third oxidation (10 mV), the latter of which displays an almost negligible effect of the electron-withdrawing NO₂Ph groups on the redox potentials.

The relative magnitude of the substituent effect should be related to the probable site of electron transfer, and the data in

Figure 3 provide strong indirect evidence for the first reduction and first oxidation of **1–4** being located on the corrole macrocycle. This contrasts with the second and third oxidations of the compounds in the two solvents, which “feel” only slightly the effect of the electron-withdrawing NO₂Ph groups, thus indicating an electron transfer site more localized on the two phthalocyanine macrocycles, which are farther removed from the corrole *meso*-NO₂Ph substituents.

The effect of NO₂Ph groups on the second reduction potentials of **2–4** in PhCN (Figure 4), CH₂Cl₂ (Figure S8),

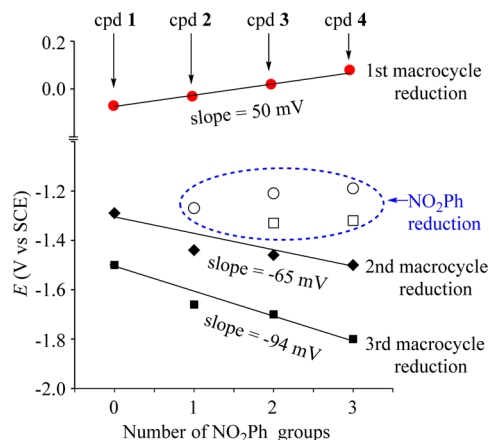


Figure 4. Plots of reduction potentials vs the number of NO₂Ph groups on compounds **1–4** in PhCN containing 0.1 M TBAP.

and pyridine (Figure S9) also provides strong indirect evidence for this electron transfer process being totally localized on a NO₂Ph substituent of the compounds. This one-electron reduction occurs at $E_{1/2} = -1.19$ to -1.27 V in PhCN (Figure 2), -1.12 to -1.21 V in pyridine (Figure S5), and $E_{pc} = -1.26$ to -1.40 V in CH₂Cl₂ (Figure S4), values which are almost identical to the measured half-wave potentials for the one-electron reduction of unlinked nitrobenzene under the same solution conditions (see Figure S6). The third reduction of compounds **3** and **4** also involves the NO₂Ph groups on the compounds. These processes occur at ca. -1.41 V in CH₂Cl₂, -1.33 V in PhCN, and -1.29 V in pyridine (see Table 2).

The last two reductions of compounds **2**, **3**, and **4** are assigned to electron additions at the corrole or phthalocyanine π ring system (as opposed to the redox-active nitrobenzene substituents), and the negative shift of $E_{1/2}$ shown in Figure 4 with increasing number of NO₂Ph groups for these two processes can be accounted for by the increasing negative charge on the molecules with each conversion of a *meso*-NO₂Ph substituent to its [NO₂Ph][−] form.

In summary, the data analysis in Figures 3 and 4 provides strong indirect evidence for assigning the probable site of electron transfer in the first two one-electron reductions and first three one-electron oxidations of compounds **1–4**. Two additional pieces of evidence are given in support of these assignments. The first involves a relationship between the measured potentials for oxidation or reduction and the Hammett substituent constants associated with the nitro groups on the corrole (Figure 5). The second involves an analysis of UV–visible spectra for the electroreduced or electrooxidized species obtained by thin-layer UV–visible spectro-electrochemistry.

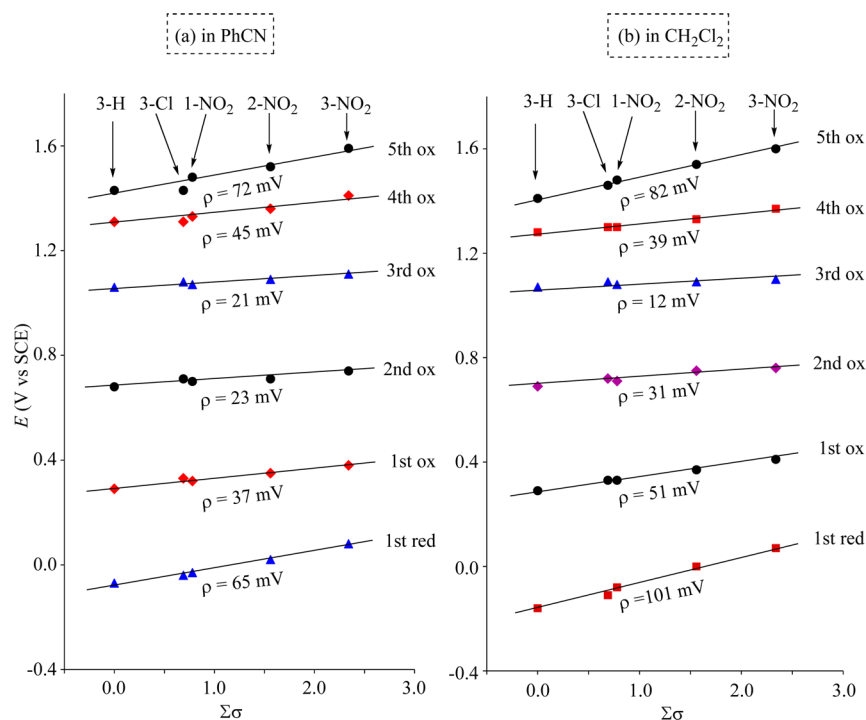


Figure 5. Plots of the redox potentials (a) PhCN and (b) CH_2Cl_2 containing 0.1 M TBAP vs the sum of the Hammett substituent constants ($\Sigma\sigma$) for the triple-decker complexes containing Cl, H, or NO_2 groups on the *para* positions of the *meso*-phenyl rings of the corrole macrocycle. The Hammett substituent constants are taken from ref 68.

The effect of electron-donating or electron-withdrawing substituents on half-wave potentials for oxidation or reduction of compounds 1–4 can be quantified by the use of eq 1,^{68,69} where σ is the electron-donating or electron-withdrawing characteristic of the substituent,⁷⁰ and ρ is the magnitude of the interaction between the substituent and the site of electron transfer. The larger the value of ρ , the larger the effect of the substituents on the reaction site. A plot $E_{1/2}$ versus $\Sigma\sigma$ can then be used to suggest the site of electron transfer in much the same way as the plots in Figures 3 and 4.

$$\Delta E_{1/2} = \Sigma\sigma\rho \quad (1)$$

A plot of the measured potentials for the first reduction and five oxidations of compounds 1–4 is given in Figure 5. Also included in this figure are potentials for the same six redox reactions of $\text{Eu}_2[\text{Pc}(\text{OC}_4\text{H}_9)_8]_2[\text{Cor}(\text{PhCl})_3]$ 5, which possesses a ClPh substituent at the three *meso* positions of the corrole macrocycle.

The values of ρ for ring-centered reductions or oxidations of porphyrins and corroles with phenyl-substituted groups at the *meso* positions of the macrocycle generally range from 30 to 50 mV for monomeric compounds.⁶⁹ Much smaller values of ρ are sometimes observed when the reaction site is farther removed from the electron-donating or electron-withdrawing substituents, a good example being in the case of metal-centered redox reactions. With this in mind, one can use the linear free-energy relationships in Figure 5 as a diagnostic criteria to propose the probable initial site of electron transfer in each redox reaction. A relatively large value of ρ will suggest a redox reaction at the corrole macrocycle containing the substituents, and a relatively small value of ρ will suggest a reaction at the phthalocyanine macrocycles, which are farther removed from the electron-withdrawing NO_2Ph substituents and separated from the corrole ligand by a europium ion.

The data in Figure 5 are consistent with the linear free-energy relationships illustrated in Figures 3 and 4. The largest value of ρ (101 mV) is observed for the first reduction of the compounds in CH_2Cl_2 , and this process is assigned as electron addition to the corrole macrocycle on the basis of the large ρ value. The smallest value of ρ is seen for the third oxidation of the compounds in CH_2Cl_2 (12 mV), and this process is assigned as involving electron abstraction from one or both of the Pc macrocycles. The ρ for the first oxidation of the five compounds in Figure 5 is 51 mV in CH_2Cl_2 compared to 31 mV for the second oxidation in this solvent. This is also consistent with assignment of electron abstraction from the corrole macrocycle in the first oxidation.

A similar comparison of ρ values can be made for the data in PhCN where the slopes are 37 and 23 mV for the first and second oxidations, respectively. This also suggests an oxidation at the corrole macrocycle, but, as shown by the spectro-electrochemical data described below, this process also has some characteristics of a Pc-based electron abstraction.

The spectral changes that occur during the first controlled reduction of 1–4 in PhCN are illustrated in Figure 6 and are the most definitive in terms of assigning the probable site of electron addition. The band at 421–439 nm is attributed to the corrole Soret band. The fact that this band significantly decreases in intensity after the addition of one electron is consistent with electron addition to the π -ring system of the corrole and also fits with the very large ρ values in Figure 5. Also consistent with assignment of reaction at the corrole is the fact that the phthalocyanine Q-band at 675–683 nm shifts to 622–647 nm but remains relatively unchanged in intensity. This latter change indicates a reduction that is not located prominently on the π -ring system of the phthalocyanine macrocycles; however, note that the singly reduced species has

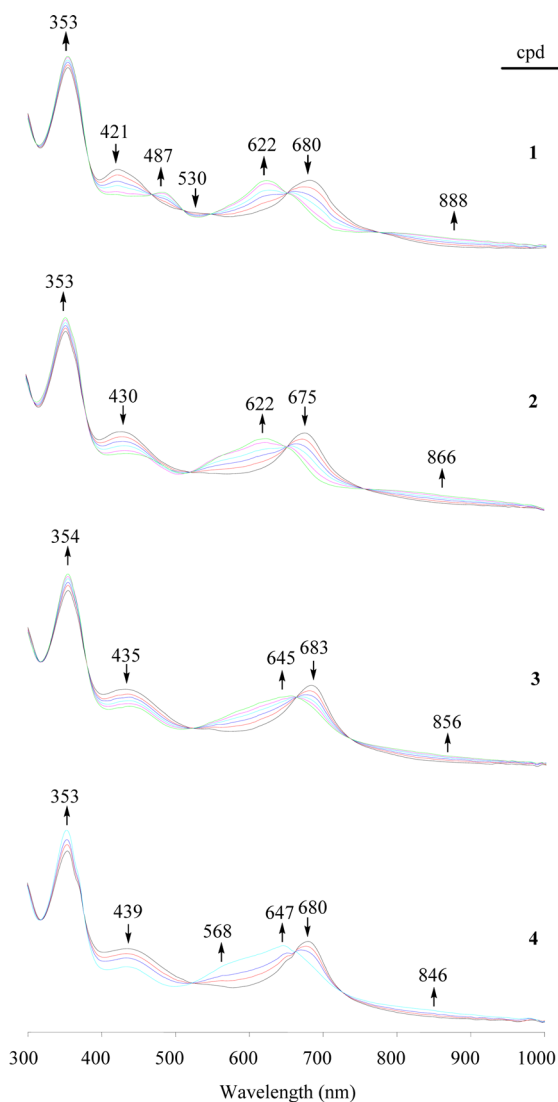


Figure 6. UV-vis spectral changes during the first controlled potential reduction of compounds 1–4 at -0.60 V in PhCN containing 0.1 M TBAP.

a broad band from 700 to 950 nm, which could indicate some radical character.

The Q-band assigned to the phthalocyanine macrocycle at 676 – 683 nm remains well-defined after the first controlled potential oxidation of compounds 1–4 but decreases in intensity. This is illustrated in Figure 7 for the case of 1 and Figure S10 for 2 and 3, where the controlled potential oxidation was performed at $+0.50$ V (compounds 1 and 2) or $+0.60$ V (compound 3). The 353 – 356 nm band assigned to the Pc macrocycle also decreases slightly in intensity during the first oxidation of 1–4, thus suggesting some degrees of positive charge on the Pc macrocycles.

The second oxidation of 1–4 was assigned on the basis of the linear free-energy relationships in Figures 3 and 5 as occurring predominantly at the Pc ligands, and the same conclusion can be reached by the significant loss in intensity of the Q-band during the second oxidation of compounds 1 (Figure 7), 2 (Figure S10), and 3 (Figure S10). The Q-band of these triple-decker compounds as well as the band at ~ 350 nm are both further reduced in intensity after the third oxidation,

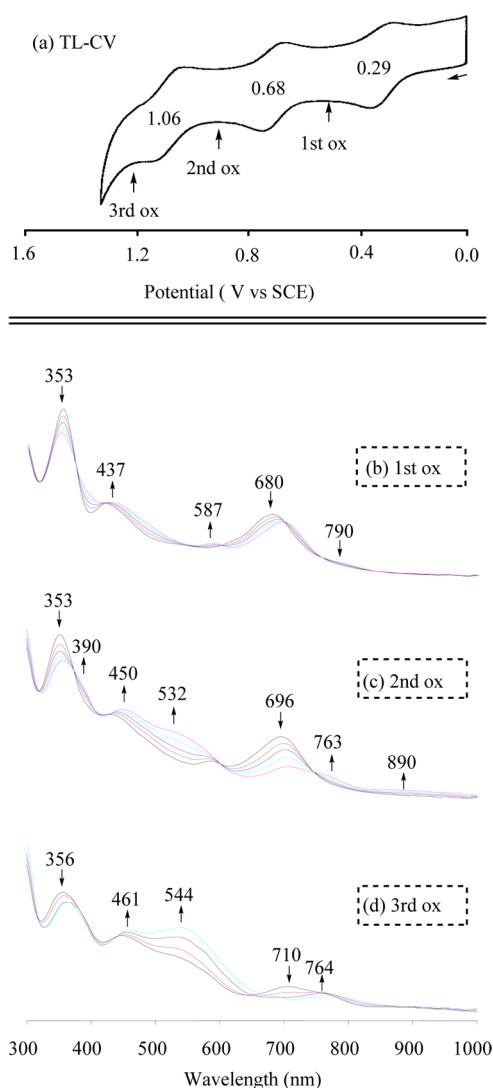


Figure 7. (a) Thin-layer cyclic voltammogram of $\text{Eu}_2[\text{Pc}(\text{OC}_4\text{H}_9)_8]_2\text{[Cor(Ph)}_3\text{]}_1$ in PhCN containing 0.1 M TBAP and UV-vis spectral changes during the first three controlled potential one-electron oxidations at (b) 0.50 , (c) 0.90 , and (d) 1.25 V.

and this reaction can also be assigned as occurring at the Pc macrocycles of 1–4 on the basis of these changes.

In summary, a new series of europium triple-decker complexes containing two phthalocyanine and one nitrophenyl-substituted corrole macrocycle was synthesized and characterized by spectroscopic and electrochemical methods in three different nonaqueous solvents. One of the compounds was also structurally characterized. The investigated compounds can be reversibly oxidized in five one-electron transfer steps, and they can also be reduced in 3–5 one-electron transfer steps, giving triple-decker complexes in up to 11 different oxidation states. The potentials for oxidation and reduction will depend upon the number and nature of substituents on both the corrole and phthalocyanine macrocycles. In this paper, we have only investigated substituent effects related to the corrole, but new compounds with different phthalocyanine substituents are also possible and will be considered in future studies.

■ ASSOCIATED CONTENT

■ Supporting Information

The Supporting Information is available free of charge on the ACS Publications website at DOI: 10.1021/acs.inorgchem.5b01713. CCDC 1411324 for 3, containing the supplementary crystallographic data for this paper, can be obtained free of charge from the Cambridge Crystallographic Data Centre via www.ccdc.cam.ac.uk/data_request/cif.

MALDI-TOF mass spectra, IR spectra, cyclic voltammograms, electronic absorption spectrum, plots of redox potentials versus the number of NO₂Ph groups on compounds, thin-layer cyclic voltammograms and UV-vis spectral changes during the first three one-electron controlled potential oxidations, selected bond distances and angles. (PDF)

Crystallographic data for Eu₂[Pc(OC₄H₉)₈]₂[Cor(Ph)(NO₂Ph)₂]. (CIF)

■ AUTHOR INFORMATION

Corresponding Authors

*E-mail: luguifen@ujs.edu.cn. (G.L.)

*E-mail: kkadish@uh.edu. (K.M.K.)

Notes

The authors declare no competing financial interest.

■ ACKNOWLEDGMENTS

The authors thank the National Natural Science Foundation of China (Nos. 21001054 and 21071067), the Foundation of Jiangsu Univ. (09JDG055), and the Robert A. Welch Foundation (K.M.K., Grant No. E-680). We are also thankful for the support of the China Council Scholarship.

■ REFERENCES

- (1) Buchler, J. W.; Ng, D. K. P. In *The Porphyrin Handbook*; Kadish, K. M., Smith, K. M., Guillard, R., Eds.; Academic Press: San Diego, CA, 2000; Vol. 3, pp 245–294.
- (2) Weiss, R.; Fischer, J. In *The Porphyrin Handbook*; Kadish, K. M., Smith, K. M., Guillard, R., Eds.; Academic Press: San Diego, CA, 2003; Vol. 16, pp 171–246.
- (3) Jiang, J.; Ng, D. K. P. *Acc. Chem. Res.* **2009**, *42*, 79–88.
- (4) Bian, Y.; Zhang, Y.; Ou, Z.; Jiang, J. In *Handbook of Porphyrin Science*; Kadish, K. M., Smith, K. M., Guillard, R., Eds.; World Scientific Publishing Co.: Singapore, 2011; Vol. 14, pp 249–460.
- (5) Bouvet, M.; Gaudillat, P.; Suisse, J.-M. *J. Porphyrins Phthalocyanines* **2013**, *17*, 628–635.
- (6) Pushkarev, V. E.; Tomilova, L. G.; Tomilov, Y. V. *Russ. Chem. Rev.* **2008**, *77*, 875–907.
- (7) Kan, J.; Chen, Y.; Qi, D.; Liu, Y.; Jiang, J. *Adv. Mater.* **2012**, *24*, 1755–1758.
- (8) Sakaue, S.; Fuyuhiko, A.; Fukuda, T.; Ishikawa, N. *Chem. Commun.* **2012**, *48*, 5337–5339.
- (9) Sheng, N.; Zhu, P.; Ma, C.; Jiang, J. *Dyes Pigm.* **2009**, *81*, 91–96.
- (10) Tanaka, H.; Ikeda, T.; Takeuchi, M.; Sada, K.; Shinkai, S.; Kawai, T. *ACS Nano* **2011**, *5*, 9575–9582.
- (11) Kong, X.; Zhang, X.; Gao, D.; Qi, D.; Chen, Y.; Jiang, J. *Chem. Sci.* **2015**, *6*, 1967–1972.
- (12) Gao, J.; Lu, G.; Kan, J.; Chen, Y.; Bouvet, M. *Sens. Actuators, B* **2012**, *166–167*, 500–507.
- (13) Lu, J.; Ma, P.; Zhang, X.; Jiang, J. *Dalton Trans.* **2011**, *40*, 12895–12900.
- (14) Lu, G.; Chen, Y.; Zhang, Y.; Bao, M.; Bian, Y.; Li, X.; Jiang, J. *J. Am. Chem. Soc.* **2008**, *130*, 11623–11630.
- (15) Gross, T.; Chevalier, F.; Lindsey, J. S. *Inorg. Chem.* **2001**, *40*, 4762–4774.
- (16) Gao, D.; Zhang, X.; Kong, X.; Chen, Y.; Jiang, J. *ACS Appl. Mater. Interfaces* **2015**, *7*, 2486–2493.
- (17) Gao, D.; Zhang, X.; Luan, J.; Chen, Y. *Inorg. Chem. Commun.* **2015**, *54*, 50–53.
- (18) Chen, Y.; Su, W.; Bai, M.; Jiang, J.; Li, X.; Liu, Y.; Wang, L.; Wang, S. *J. Am. Chem. Soc.* **2005**, *127*, 15700–15701.
- (19) Kan, J.; Wang, H.; Sun, W.; Cao, W.; Tao, J.; Jiang, J. *Inorg. Chem.* **2013**, *52*, 8505–8510.
- (20) Morita, T.; Katoh, K.; Breedlove, B. K.; Yamashita, M. *Inorg. Chem.* **2013**, *52*, 13555–13561.
- (21) Lysenko, A. B.; Malinovskii, V. L.; Padmaja, K.; Wei, L.; Diers, J. R.; Bocian, D. F.; Lindsey, J. S. *J. Porphyrins Phthalocyanines* **2005**, *9*, 491–508.
- (22) Chabach, D.; De Cian, A.; Fischer, J.; Weiss, R.; Bibout, M. E. *Angew. Chem., Int. Ed. Engl.* **1996**, *35*, 898–899.
- (23) Katoh, K.; Asano, R.; Miura, A.; Horii, Y.; Morita, T.; Breedlove, B. K.; Yamashita, M. *Dalton Trans.* **2014**, *43*, 7716–7725.
- (24) Huang, W.; Xiang, H.; Gong, Q.; Huang, Y.; Huang, C.; Jiang, J. *Chem. Phys. Lett.* **2003**, *374*, 639–644.
- (25) Zhu, P.; Pan, N.; Ma, C.; Sun, X.; Arnold, D. P.; Jiang, J. *Eur. J. Inorg. Chem.* **2004**, *2004*, 518–523.
- (26) Sun, X.; Li, R.; Wang, D.; Dou, J.; Zhu, P.; Lu, F.; Ma, C.; Choi, C.-F.; Cheng, D. Y. Y.; Ng, D. K. P.; Kobayashi, N.; Jiang, J. *Eur. J. Inorg. Chem.* **2004**, *2004*, 3806–3813.
- (27) Sun, X.; Cui, X.; Arnold, D. P.; Choi, M. T. M.; Ng, D. K. P.; Jiang, J. *Eur. J. Inorg. Chem.* **2003**, *2003*, 1555–1561.
- (28) Gryko, D.; Li, J.; Diers, J. R.; Roth, K. M.; Bocian, D. F.; Kuhr, W. G.; Lindsey, J. S. *J. Mater. Chem.* **2001**, *11*, 1162–1180.
- (29) Li, J.; Gryko, D.; Dabke, R. B.; Diers, J. R.; Bocian, D. F.; Kuhr, W. G.; Lindsey, J. S. *J. Org. Chem.* **2000**, *65*, 7379–7390.
- (30) Padmaja, K.; Youngblood, W. J.; Wei, L.; Bocian, D. F.; Lindsey, J. S. *Inorg. Chem.* **2006**, *45*, 5479–5492.
- (31) Schweikart, K.-H.; Malinovskii, V. L.; Yasseri, A. A.; Li, J.; Lysenko, A. B.; Bocian, D. F.; Lindsey, J. S. *Inorg. Chem.* **2003**, *42*, 7431–7446.
- (32) Martynov, A. G.; Zubareva, O. V.; Gorbunova, Y. G.; Sakharov, S. G.; Nefedov, S. E.; Dolgushin, F. M.; Tsivadze, A. Y. *Eur. J. Inorg. Chem.* **2007**, *2007*, 4800–4807.
- (33) Birin, K. P.; Gorbunova, Y. G.; Tsivadze, A. Y. *Dalton Trans.* **2012**, *41*, 9672–9681.
- (34) Lei, S.-B.; Deng, K.; Yang, Y.-L.; Zeng, Q.-D.; Wang, C.; Jiang, J.-Z. *Nano Lett.* **2008**, *8*, 1836–1843.
- (35) Lu, J.; Deng, Y.; Zhang, X.; Kobayashi, N.; Jiang, J. *Inorg. Chem.* **2011**, *50*, 2562–2567.
- (36) Lu, G.; Yan, S.; Shi, M.; Yu, W.; Li, J.; Zhu, W.; Ou, Z.; Kadish, K. M. *Chem. Commun.* **2015**, *51*, 2411–2413.
- (37) Paolesse, R. In *The Porphyrin Handbook*; Kadish, K. M., Smith, K. M., Guillard, R., Eds.; Academic Press: San Diego, CA, 2000; Vol. 2, pp 201–232.
- (38) Erben, C.; Will, S.; Kadish, K. M. In *The Porphyrin Handbook*; Kadish, K. M., Smith, K. M., Guillard, R., Eds.; Academic Press: San Diego, CA, 2000; Vol. 2, pp 233–300.
- (39) Lu, G.; Li, J.; Yan, S.; Zhu, W.; Ou, Z.; Kadish, K. M. *Inorg. Chem.* **2015**, *54*, 5795–5805.
- (40) Lu, G.; Li, J.; Yan, S.; He, C.; Shi, M.; Zhu, W.; Ou, Z.; Kadish, K. M. *Dyes Pigm.* **2015**, *121*, 38–45.
- (41) Gryko, D. T. *Eur. J. Org. Chem.* **2002**, *2002*, 1735–1743.
- (42) Stefanelli, M.; Nardis, S.; Tortora, L.; Fronczek, F. R.; Smith, K. M.; Licoccia, S.; Paolesse, R. *Chem. Commun.* **2011**, *47*, 4255–4257.
- (43) Steene, E.; Wondimagegn, T.; Ghosh, A. *J. Phys. Chem. B* **2001**, *105*, 11406–11413.
- (44) Ghosh, A.; Steene, E. *J. Inorg. Biochem.* **2002**, *91*, 423–436.
- (45) Pacholska, E.; Espinosa, E.; Guillard, R. *Dalton Trans.* **2004**, *3181–3183*.
- (46) Teo, R. D.; Gray, H. B.; Lim, P.; Termini, J.; Domeshek, E.; Gross, Z. *Chem. Commun.* **2014**, *50*, 13789–13792.
- (47) Gross, Z. *JBIC, J. Biol. Inorg. Chem.* **2001**, *6*, 733–738.

- (48) Nardis, S.; Cicero, D. O.; Licoccia, S.; Pomarico, G.; Berionni Berna, B.; Sette, M.; Ricciardi, G.; Rosa, A.; Fronczek, F. R.; Smith, K. M.; Paolesse, R. *Inorg. Chem.* **2014**, *53*, 4215–4227.
- (49) Aviv-Harel, I.; Gross, Z. *Chem. - Eur. J.* **2009**, *15*, 8382–8394.
- (50) Flamigni, L.; Gryko, D. T. *Chem. Soc. Rev.* **2009**, *38*, 1635–1646.
- (51) Aviv-Harel, I.; Gross, Z. *Coord. Chem. Rev.* **2011**, *255*, 717–736.
- (52) Liu, H.-Y.; Mahmood, M. H. R.; Qiu, S.-X.; Chang, C. K. *Coord. Chem. Rev.* **2013**, *257*, 1306–1333.
- (53) Paolesse, R. *Synlett* **2008**, *2008*, 2215–2230.
- (54) Thomas, K. E.; Alemayehu, A. B.; Conradie, J.; Beavers, C. M.; Ghosh, A. *Acc. Chem. Res.* **2012**, *45*, 1203–1214.
- (55) Buckley, H. L.; Anstey, M. R.; Gryko, D. T.; Arnold, J. *Chem. Commun.* **2013**, *49*, 3104–3106.
- (56) Stefanelli, M.; Mandoj, F.; Mastroianni, M.; Nardis, S.; Mohite, P.; Fronczek, F. R.; Smith, K. M.; Kadish, K. M.; Xiao, X.; Ou, Z.; Chen, P.; Paolesse, R. *Inorg. Chem.* **2011**, *50*, 8281–8292.
- (57) Nardis, S.; Stefanelli, M.; Mohite, P.; Pomarico, G.; Tortora, L.; Manowong, M.; Chen, P.; Kadish, K. M.; Fronczek, F. R.; McCandless, G. T.; Smith, K. M.; Paolesse, R. *Inorg. Chem.* **2012**, *51*, 3910–3920.
- (58) Li, B.; Ou, Z.; Meng, D.; Tang, J.; Fang, Y.; Liu, R.; Kadish, K. M. *J. Inorg. Biochem.* **2014**, *136*, 130–139.
- (59) Fang, Y.; Jiang, X.; Ou, Z.; Michelin, C.; Desbois, N.; Gros, C. P.; Kadish, K. M. *J. Porphyrins Phthalocyanines* **2014**, *18*, 832–841.
- (60) Chen, Y.; Liu, H.-G.; Zhu, P.; Zhang, Y.; Wang, X.; Li, X.; Jiang, J. *Langmuir* **2005**, *21*, 11289–11295.
- (61) Stites, J. G.; McCarty, C. N.; Quill, L. L. *J. Am. Chem. Soc.* **1948**, *70*, 3142–3.
- (62) Zhu, P.; Pan, N.; Li, R.; Dou, J.; Zhang, Y.; Cheng, D. Y. Y.; Wang, D.; Ng, D. K. P.; Jiang, J. *Chem. - Eur. J.* **2005**, *11*, 1425–1432.
- (63) Chabach, D.; Lachkar, M.; De Cian, A.; Fischer, J.; Weiss, R. *New J. Chem.* **1992**, *16*, 431–3.
- (64) Jiang, J.; Bian, Y.; Furuya, F.; Liu, W.; Choi, M. T. M.; Kobayashi, N.; Li, H.-W.; Yang, Q.; Mak, T. C. W.; Ng, D. K. P. *Chem. - Eur. J.* **2001**, *7*, 5059–5069.
- (65) Lv, W.; Zhu, P.; Bian, Y.; Ma, C.; Zhang, X.; Jiang, J. *Inorg. Chem.* **2010**, *49*, 6628–6635.
- (66) Lu, G.; Bai, M.; Li, R.; Zhang, X.; Ma, C.; Lo, P.-C.; Ng, D. K. P.; Jiang, J. *Eur. J. Inorg. Chem.* **2006**, *2006*, 3703–3709.
- (67) Zhang, Y.; Jiang, W.; Jiang, J.; Xue, Q. *J. Porphyrins Phthalocyanines* **2007**, *11*, 100–108.
- (68) Zuman, P. *Substituent Effects in Organic Polarography* **1967**, 169.
- (69) Kadish, K. M.; Caemelbecke, E.; Van, R. G. In *The Porphyrin Handbook*; Kadish, K. M., Smith, K. M., Guillard, R., Eds.; Academic Press: San Diego, CA, 2000; Vol. 8, pp 1–114.
- (70) Hansch, C.; Leo, A.; Taft, R. W. *Chem. Rev.* **1991**, *91*, 165–95.